Influence of doping novel perimidine ruthenium complexes on structural, optic, and residual stress properties of ZnO thin films

Abuzer Acikgoz (a.abuzer@harran.edu.tr)
Harran University https://orcid.org/0000-0002-2648-3560
Gokhan Demircan
Harran University
Serife Yalcin
Harran University
Emine Aytar
Harran University
Mehmet Vehbi Balak
Harran University
Bulent Aktas
Harran University

Research Article

Keywords: ZnO thin films, Ruthenium complexes, Residual stress, Spin coating method, Sol-gel

Posted Date: April 12th, 2022

DOI: https://doi.org/10.21203/rs.3.rs-1533241/v1

Version of Record: A version of this preprint was published at Brazilian Journal of Physics on December 14th, 2022. See the published version at https://doi.org/10.1007/s13538-022-01245-x.

Abstract

Novel perimidine ruthenium complexes ([Ru(L1-2)(p-cymene)Cl]Cl) were synthesized and these synthesized Ruthenium (Ru) complexes were added to ZnO at content of 2, 4, 6 wt.% to fabricate Ru-doped ZnO thin films by the sol-gel spin-coating method. These films were characterized using XRD, SEM, FT-IR, UV-Vis, and Photoluminescence (PL) spectra. All of the films possessed a hexagonal wurtzite structure, according to XRD data. The observed stress was compressive, except for the A4 sample, and ranged from 0.21 GPa to 2.117 GPa as the ruthenium content increased from 0–6%. Residual stress values of Ru-doped ZnO thin films showed a lower value than pure ZnO film. It was obtained that the crystalline quality tended to improve as well as lower residual stress with increasing Ru amount. In the visible range, all the films exhibited approximately transmittance greater than 70%. Further, the optical bandgap was 3.20 eV for pure ZnO and all Ru-doped films' bandgap had between 2.76 and 3.18 eV. This research shows that new high conjugated structures are promising as dopant materials for the ZnO thin film, and good crystalline and optical properties could be obtained from the Ru doped ZnO films prepared by sol-gel for nano-optoelectronic devices.

1. Introduction

Zinc oxide (ZnO) is a multifunctional semiconductor oxide that is used in a variety of applications due to its unique characteristics and a variety of applications, such as microelectronic devices [1], sensors [2], batteries [3] and optoelectronics [4]. It is a desirable substance for material science due to its wide energy band (3.37 eV), high bond energy (60 meV) and elevated thermal and mechanical performance at room temperature [5]. Doped and undoped zinc oxide is used in sol-gel derived thin film production, and it attracts scientists’ attention due to structural, optical and electrical properties [6–8]. The dopant materials are used to improve electrical, structural, optical, etc. properties of ZnO thin films [9]. In production of ZnO thin films, there are a lot of obtained methods such as evaporation [10], sputtering [11], pulsed laser deposition [12], sol-gel [13] and chemical bath deposition [14]. Among these methods, the most preferred one is sol-gel which has simple stages of (i) exhausting, (ii) excess deposit processing, and (iii) drying, provides good control over the chemical composition with low temperature, low cost and low energy consumption [15].

Ruthenium (Ru) is one of the dopant materials used to produce ZnO thin film. It's an unique transition metal that's part of the platinum group on the periodic chart (PGMs). Ruthenium is extremely scarce as the 74th most common ingredient of the Earth's crust, occurring in around 0.001 ppm [16]. This element is commonly present in ores in the Ural Mountains and in North and South America, along with the other platinum group metals such as Osmiridium, Iridiosmium and Laurite [17]. This metal is used in a number of fields, such as the medicine, mechanical and chemical industries [18, 19]. It has special chemical and physical characteristics, such as high conductivity, high melting point, hardness and catalytic effects. Due to these outstanding properties, ruthenium is used as a dopant material in the production of thin films.

There are several Ru compounds in the literature. Ruthenium (III) chloride is one of them and used to produce Ru-doped ZnO thin films in some studies [20–23]. Vettumperumal et al. [20] prepared nanocrystalline Ru-doped ZnO thin film using sol-gel spin-coating with Ruthenium (III) chloride and investigated structural properties and UV characteristics. They observed an improvement in sheet resistance with an increase in the dopant amount of Ru (1–2 mol%) and recorded an improved I-V characteristic response at 1 mol% of thin films. Gómez-Pozos et al. [21] deposited ruthenium and chromium-doped zinc oxide thin films using sol-gel dip-coating on soda-lime glass substrates for gas sensing application. They used Ruthenium (III) chloride for Ru-doped thin film with a non-alkoxide route. The doping process was done as one, three, and five immersions. They observed that Ru was better than Cr in five immersions for C_3H_8 gas detection.

Besides the commercially available Ruthenium (III) chloride, there are Ruthenium complex compounds that have notable growth and improvement in the area of coordination and organometallic chemistry. Recently, several publications have appeared on the creation and applications of Ru-based complexes in fields such as nanoscience, catalysis, medicine, genetics, redox and photoactive materials. The fact that Ru has outstanding potential to appear in several oxidation states may be connected to these advances. Three key properties of ruthenium-based complexes have been stated by Claire et al. [24] to make them suitable for drug application. Lida et al [25] explored the role of ruthenium complexes on cancer inhibitory activity. Li et al. [26] investigated the antimicrobial activity of ruthenium complexes and discussed the relationship between biological processing and chemical composition. Although there are several studies related to different application areas, there is no study related to ZnO thin film produced by using Ruthenium complex compounds. The aim of this study is to investigate the usability of Ruthenium complex compounds in ZnO thin films. These complex compounds were synthesized using high conjugation perimidine ligand system (L_1 and L_2) as mentioned previously published procedures [27–30].

The incorporation of Ru into ZnO at nanoscale sizes can change the stress in the lattice of ZnO as a result of the tensile or compressive stress occurring in the nanostructured films formed with Ru doping [31]. For this reason, we synthesized novel perimidine ruthenium complexes ([Ru(L1-2)(p-cymene)Cl]Cl) derived from 2-pyridinecarboxaldehyde/quinoline-2-carboxaldehyde and 1,8-diaminonaphthalene, and these Ru-complexes were added to ZnO at content of 2, 4, 6 wt.% to fabricate Ru-doped ZnO thin films by the sol-gel spin-coating method. The stress measurements of the fabricated films were performed with the XRD method, and compared with the crystal sizes obtained from SEM and XRD. Furthermore, structural and optical properties of Ru-doped ZnO thin films were investigated by FTIR, UV-vis, and PL spectra.

2. Experimental Procedure

2.1. Synthesis of ligands and [Ru(L_{1-2})(*p*-cymene)Cl]Cl complex compounds

The all ligands and metal complexes were synthesized with high yield. As summarized in Fig. 1, with the optimized conditions in hand,ligands (L_{1-2}) were prepared in moderate yield by one pot reaction via 1,8-diaminonaphthalene refluxing the 1:1 molar ratio of with 2-pyridinecarboxaldehyde and 2-quinolinecarboxaldehyde in anhydrous ethanol (EtOH).

The targeted ligands (L1-2) were produced in good yields as solids upon recrystallization (80–85%), and all ligands had satisfactory spectroscopic results. As summarized in Scheme 1, the metal complexes ([Ru(L_{1-2})(*p*-cymene)Cl]Cl) were obtained by reactions of ligands (L_{1-2}) with $[RuCl_2(p\text{-cymene})]_2$ in good yields as yellow solids following recrystallization. All attempts for the X-Ray quality crystals were failed. The synthesis and spectroscopic data of the ligands (L_{1-2}) and their metal complexes ([Ru(L_{1-2})(*p*-cymene)Cl]Cl) were given as supporting information. The ^{1}H and ^{13}C NMR spectra and LC MS/MS with elemental analysis results support 1:1 ratio of metal/ligand, as expect. The ligands and their compounds confirmed the indicated structures, according to multinuclear NMR spectra and elemental analyses.

2.2. Preparation of Ru-doped ZnO thin films

Sol-gel spin-coating was used to synthesize Ru-doped ZnO thin films on a glass substrate. The starting material and stabilizer were zinc acetate dihydrate $[Zn(CH_3COO)_2.2H_2O]$ and monoethanolamine (MEA). Ethanol, dimethyl sulfoxide (DMSO) and isopropanol were used as the solvent. Commercially available Ruthenium (III) chloride ($RuCl_3 \cdot xH_2O$), synthesized [Ru(L_{1-2})(*p*-cymene)Cl]Cl complexes were used as dopant materials. The first step is to dissolve the Zinc acetate dihydrate in a mixture of MEA and isopropanol. Zinc acetate had a molar content of 0.5 M. The molar ratio of monoethanolamine to zinc acetate was kept constant at 1:1. Using a magnetic stirrer, the solution was first stirred at 65 C for 30 min to get a clear and uniform sol. At this stage, ruthenium solutions were added to the zinc acetate solution and mixed for another 90 min. Ruthenium solutions were prepared by dissolving ruthenium compounds in 20 µl DMSO and 0.5 ml ethanol. Three different dopant concentrations (2, 4, 6 wt.% with respect to zinc acetate) were used. The notations of nine different thin films are shown in Table 1.

Table 1
ZnO thin film notations

Notations	Thin film	Dopant	Dopant concentration
Z0	ZnO	Undoped	0 wt.%
A2	ZnO	$RuCl_3 \cdot xH_2O$	2 wt.%
A4	ZnO	$RuCl_3 \cdot xH_2O$	4 wt.%
A6	ZnO	$RuCl_3 \cdot xH_2O$	6 wt.%
B2	ZnO	[Ru(L_1)(*p*-cymene)Cl]Cl	2 wt.%
B4	ZnO	[Ru(L_1)(*p*-cymene)Cl]Cl	4 wt.%
B6	ZnO	[Ru(L_1)(*p*-cymene)Cl]Cl	6 wt.%
C2	ZnO	[Ru(L_2)(*p*-cymene)Cl]Cl	2 wt.%
C4	ZnO	[Ru(L_2)(*p*-cymene)Cl]Cl	4 wt.%
C6	ZnO	[Ru(L_2)(*p*-cymene)Cl]Cl	6 wt.%

The final solutions were aged at room temperature for 24 h. Before the deposition process, the glass substrates were washed with soapy water and ultrasonically cleaned to remove any dirt, oil and grease in deionized water, isopropanol and acetone for 10 minutes each, respectively. The thin films were prepared using a spin coater (POLOS SPIN200i-NPP-INT) at 3000 rpm and 30 s, followed by a 10 min drying process at 200°C on a hot plate to extract solvents. The deposition and drying procedures were repeated 10 times to get a thin film. Finally, the films were annealed at 450°C for 1 h in a furnace at air atmosphere. The flow chart for the deposition procedure of Ru-doped ZnO thin films is shown in Fig. 2.

2.3. Characterization of Ru-doped ZnO thin films

X-Ray Diffraction (XRD) studies were performed to obtain the information of phases, crystalline quality and the crystallite size. CuK alpha radiation was used to do the tests (Rigaku Dmax 2000 Diffractometer) at 40 kV and 30 mA. The range of 2θ scanning speed (0.02) was performed from 20° to 70°. All measurements were done on coated surfaces of glasses. Residual stress analyses were performed using $\sin^2\psi$ method. Rietveld refinements were conducted using match software. Optical transmission spectra, were conducted with a scanning speed of 0.02 in a 200–800 nm wavelength range (Shimadzu UV-1700). The surface characteristics and thickness measurements of the films were analyzed using a SEM microscope (Zeiss Evo 50). Photoluminescence (PL) measurements were carried out using a spectrometer at room temperature (Perkin Elmer LS 55) with a Xenon flash lamp (at line frequency 50 or 60 Hz) as an excitation source in the range of 200 to 800 nm with a step of 1 nm. FT-IR spectra in the

range of 4000 – 400 cm^{-1} were acquired using a Perkin Elmer Two UATR-FT-IR spectrophotometer and the ATR accessory with a diamond ATR crystal.

3. Result And Discussion

3.1 XRD analysis

Figure 3 displays the XRD patterns of the deposited Ru-doped ZnO films. All peaks were indexed well with the zinc oxide (pdf number: 01-075-0576) or zincite (pdf number: 01-075-1526) structure with preferential orientation along (002). No diffraction peaks that belong to ruthenium are observed in all samples. The peak is a little bit wider for low content of Ru doping. But the peaks' positions slightly shift to a little bit higher 2-theta values with ruthenium entering into the matrix, and it becomes sharper with ruthenium doping. Further, an increasing tendency in the intensity of (002) and (101) peak has occurred with the increasing of Ru doped for B and C films, while an increase in the intensity of (100) and (101) peak of A films has been observed. It is known that increases in concentration attribute to an increase in film thickness [32]. The primary XRD peaks were used to derive the lattice constants a and c, which are presented in Table 2. These parameters have shown a slight difference for Ru doped samples as compared to undoped ZnO. Ghosh et al. [33] expressed that this was due to differences in the ionic radii of Zn^{2+} and Ru^{3+}. Furthermore, the results shown in Fig. 3 clearly show that the Ru complex of the L_1 ligand gave higher peaks compared to those with the L_2 ligand.

The complete width at half-maximum of the (002) reflection has been evaluated to calculate the mean crystallite size by using conventional DebyeScherrer's formula (D). The average crystallite size of the intense diffraction peak (002) is found to be 178.8, 198.3, 244.68, 244.71, 86.9, 121.1, 200.5, 85, 141.2, and 213.4 nm for Z0, A2, A4, A6, B2, B4, B6, C2, C4 and C6, respectively. Particle size increases with an increase of Ru amount. During crystal growth, different kind of dislocations or defects can be formed. The existence of defects in the formation, such as vacancies and orientation disorder, affects the lattice parameters [34]. Furthermore, samples with greater concentrations may age faster and reach peak grain size faster than those with lower amounts [35]. The Rietveld refinement has been performed by using the Zincite and Zinc Oxide structure as starting model structure. It has occurred an increase in a and c lattice parameter after Rietveld refinement. The data is given in Table 2.

The Young's modulus of films is given in the range 76–257 GPa in the literature [36]. The interval of the Young modulus can be attributed to geometrical effects result from microfabrication. Young modulus can be calculated via Eq. 1.

$$Y_{hkl} = \frac{\left[h^2 + \frac{(h+2k)^2}{3} + (\frac{al}{c})^2\right]^2}{s_{11}(h^2 + \frac{(h+2k)^2}{3})^2 + s_{33}(\frac{al}{c})^4 + (2s_{13} + s_{44})(h^2 + \frac{(h+2k)^2}{3})\left(\frac{al}{c}\right)^2)} \quad (1)$$

Here, a and c are lattice parameters, s_{11}, s_{13}, s_{33}, and s_{44} are elastic compliances of ZnO with values 7.858×10^{-12}, -2.206×10^{-12}, 6.940×10^{-12}, and 23.571×10^{-12} m^2 N^{-1} respectively [37]. The Young modulus has been found around 48 GPa for (002) plane by using Eq. 1. in our study.

Residual stress is a significant characteristic of films that has a direct impact on the conductivity and surface morphology of the film [38]. Thus, Residual stress values and properties of films have been investigated in this study. As the ruthenium content increased from 0–6%, the residual stress values ranged from 0.21 GPa to 2.117 GPa, and the measured stress was determined to be compressive except for A4. Also, 4% doped A and B films have shown an increase and, shown a decrease in 6% decrease, whereas, C film have shown opposite. It can be due to stability problems and decreasing fiber radius of C6 film. Compare to %6 doping, C6 has demonstrated the lowest residual stress value. For ZnO films, Al-Khawaja et al. [39] have found that when crystalline quality improves with film thickness, the stress concentration reduces rapidly in increasing thickness and stays unchanged. The influence of dopants on crystallinity, according to Pham et al. [38], may be described by the growing process, which can be clarified by the desorption possibility of dopant atoms, and the varied residual stresses and crystal sizes reflect the dopant size impact on the host ZnO film structure. The thermoelectric capabilities of the ZnO thin films with the least compressive stress are enhanced by its higher Power Factor value.

Residual stress values have shown a lower value than pure ZnO film. It has been discovered that as the thickness of the produced films grows, the crystalline quality improves and the residual stress decreases. These results indicate the positive effect of the perimidine ligand derivatives for this Ru-doped ZnO thin films.

Table 2
The lattice constant, young modulus and residual stress of ZnO thin films

Thin Films	Unit cell parameter (Å)	Rietveld Refinement (Å)	Young Modulus (GPa)	Residual Stress (GPa)	Film thickness (µm)
Z0	a = 3.24, c = 5.19	a = 3.24, c = 5.19	48.46	-2.177 (1.5)	1.045
A2	a = 3.22, c = 5.15	a = 3.24, c = 5.19	48.51	-0.5 (1)	1.261
A4	a = 3.23, c = 5.16	a = 3.25, c = 5.21	48.62	1.4 (1.1)	1.436
A6	a = 3.21, c = 5.13	a = 3.25, c = 5.20	48.62	-0.9 (2)	1.714
B2	a = 3.23, c = 5.17	a = 3.24, c = 5.20	48.51	-0.8 (0.9)	1.458
B4	a = 3.22, c = 5.15	a = 3.24, c = 5.20	48.51	-1.7 (0.8)	1.919
B6	a = 3.22, c = 5.16	a = 3.24, c = 5.20	48.41	-0.4 (0.1)	2.256
C2	a = 3.22, c = 5.16	a = 3.25, c = 5.22	48.41	-1.75 (0.2)	2.014
C4	a = 3.22, c = 5.12	a = 3.24, c = 5.20	48.92	-0.21 (0.9)	2.322
C6	a = 3.22, c = 5.16	a = 3.24, c = 5.20	48.41	-0.29 (1.3)	2.586

3.2. SEM analysis

The surface structure of Ru-doped ZnO thin film was shown in SEM images in Fig. 4. Images were taken at 10.00 K magnification with EHT value at 15.00 kV. The Ru-doped ZnO thin film was mechanically stable and demonstrated very strong adherence to the substrate at room temperature. After deposition, no peel or crack were observed of the thin films except for C films. In these films, a slight decrease in stability was observed from C4 to C6 films as the addition rate increased. As can be seen from the SEM images, while there is a leafy structure in undoped thin film, a nano fiber like structure was observed in Ru-doped ones and the density of this structure increased as the amount of additive increased.

The nano fiber like structures were shown in the upper right corner for each sample SEM image in Fig. 4. The average diameters of these fibers calculated by taking different measurements were shown in Table

3. The coating thicknesses of thin films were obtained from the SEM image of the cross-sectional area. The coating thickness and fiber thickness were demonstrated in Fig. 5. Both increased as the doping rate increased except for C6 film. In this sample, it is was seen that as the coating thickness increased, the fiber thickness decreased. This reveals that the [Ru(L_2)(*p*-cymene)Cl]Cl compound used for the ruthenium doping process has a stability problem at 6 wt.%.

Table 3
Coating and fiber thickness of Ru-doped ZnO thin films

Thin film	Coating thickness (nm)	Fiber thickness (nm)
Z0	1 045	—
A2	1 261	318
A4	1 436	388
A6	1 714	475
B2	1 458	743
B4	1 919	969
B6	2 256	1 471
C2	2 014	259
C4	2 322	728
C6	2 586	627

3.3. UV-Vis analysis

The optical property of pure ZnO and Ru-doped ZnO films have been determined by UV–vis spectrometer from 300 to 800 nm wavelength range The UV–vis absorption spectra of various Ru doped ZnO thin films shows with a broad absorption in the ultraviolet region around 300–370 nm (Fig.6All of the films have a relatively high transmittance of more than 70% in the visible spectrum. The absorption edges have been found between 392–425 nm for all the films. The dramatic rise in absorbance at wavelengths of 300 nm, according to Ghosh et al. [40], is due to inter-band transitions near the fundamental edge. Undoped ZnO thin film has lower absorption in the visible range of the spectrum and the absorption edge increases for B and C films depending on Ru dopant. Further, the absorption wavelength increases from 403 to 417 nm and (403–420 nm) and shifted to blue. Blue emissions are often caused by impurities and imperfections in the ZnO lattice [41].

The bandgap is a key indicator in a solid's electrical conductivity and is influenced by layer thickness, degree of crystallinity, and temperature. Tauc's relationship was used to calculate the optical bandgaps of the coatings (Eq. 2).

$$(\alpha h\nu) = A\left(h\nu - E_g\right)^{1/2} \quad (2)$$

Here, A is constant, hv is photon energy, and a is absorption coefficient. Optical bandgap of all films prepared with different Ru concentrations 2%, 4%, and 6% for all films are given in Fig. 7. The optical bandgap is 3.20 eV for pure ZnO and all films have bandgap between 2.76–3.20 eV. The bandgaps of the A and B films have decreased with the increase of Ru content. The s–d and p–d contacts that lead to the bandgap cause the bandgap to shrink, making these materials more suitable for nano-optoelectronic devices [33, 42]. Because the wave patterns of the electrons coupled to the impure atoms begin to overlap as the Ru doping concentration level grows, the bandgap decreases at high doping densities. Allowable shallow states in the bandgap are created by impurities such as ruthenium dopant, and these shallow levels have very weak ionization energies [37]. Also, the film thickness and particle size have an effect on bandgap of films. Lower particle size has a higher bandgap due to quantization. The reason for the contraction in the Eg bandgap of Ru doped ZnO films may be that these films doping formed new recombination centers with lower emission energy. According to Kumar et al. [42], the smaller bandgap value in Ru doped ZnO nanorods can be related to the materials' oxygen-deficient non-stoichiometric nature. Whereas, the bandgap is a bit increased at C4, and then decreased at C6 film. The reason for the increase in Eg values in C films may be that the increased carrier concentration prevents low energy states in the transmission band and causes the Burstein-Moss effect [43, 44]. This explains the decrease in fiber thickness at the transition from C4 to C6, although fiber sizes increase as ruthenium contribution increases.

3.4. Photoluminescence analysis

Photoluminescence (PL) analysis is a non-destructive and sensitive analysis method used to examine defects in semiconductors and the energy levels of these defects. Room-temperature PL spectra of pure and Ru-doped ZnO films are given in Fig.8. The interface, surfaces, contamination levels, interface smoothness, and structural flaws in crystals can all affect photoluminescence (PL) intensity vs. wavelength [45].

Photoluminescence (PL) spectroscopy has been used to investigate the luminescence characteristics of individual and collective ZnO nanostructures [46]. It has been obtained three bands in PL spectra in our study. One excitation band have been observed around 326 nm and, it has been observed that the low-intensity and broad excitation peak centered at 471 nm corresponding to blue emission for B films. This peak level decreases depending on the Ru increase. This excitation peak is slightly shifted with the effect of annealing according to the literature [47]. At 650 nm, a red emission peak has been seen. The red PL

band has attributed either to the oxygen intermediate atoms (Oi) or the hydroxyl group (OH) due to the excess oxygen at the ZnO surface. The change from Zn interstitial (Zni) to oxygen interstitial (Oi) states caused the red emission. These kind of occurrences are most common in oxygen-rich environments. Other reports show that receiver defects associated with VZn are assumed to be responsible for deep-level emission close to 650 nm [48]. Crystal defects in ZnO are caused by the substitution of divalent Zn2 + ions with trivalent Ru3 + ions, such as zinc interstitials (Zni), zinc spaces (VZn), oxygen interstitials (Oi), and oxygen vacancies (VO) [47]. As the concentration of Ru ions increased, the intensity of UV emission increased due to the ZnO increasing the crystal's quality. The strong emissions have been observed in 6% Ru doped ZnO A, C, and B, respectively. In addition, it is thought that the study may have an effect on rapidly developing borate and obsidian glasses and improve the properties of these glasses [49, 50].

3.5 FT-IR analysis

FT-IR spectra of all synthesized thin films have been recorded in the range of 400–4000 cm^{-1} using KBr pellets and are shown in Fig. 9. The commercial ruthenium additive (A films) has caused to form new absorption peaks around 3672 cm^{-1} attributed to O–H stretching vibrations, and 1394 cm^{-1} bending vibration of O–H groups [51]. The peak observed around 2849 and 2918 cm^{-1} at Z0 film, which is attributed to CH_2 and CH groups and other associations by H–bond, has become more intense with the commercial ruthenium doping, and have shifted to 2920 and 2988 cm^{-1}, respectively. The υ(C = O) ester peak, seen around 1730 cm^{-1} for Z0 and 2% films, has disappeared with the increase in ruthenium amount. A shift occurred in the peaks observed around 1581, 1139 and 872 cm^{-1} with ruthenium addition. Sing et al. [52] have expressed that the reason why occur a shift in peaks of Zn–O stretching vibrations with the increasing doping of Ru, might be due to the increased replacement of Zn^{2+} ions by Ru^{3+} ions as the percentage of Ru increases in the ZnO lattice. The peaks have been observed at 2920, 2846, 1571, 1080, and 867 cm^{-1} in the spectrum of C films, similar to Z0 films. Unlike Z0 films, there has been an increase in the intensity of the peaks seen at 2920 and 2846 cm^{-1}, and the peak at 1137 cm^{-1} has shifted towards 1080 cm^{-1}. The new peaks have been observed around 3672, 1377, 1056, and 665 cm^{-1} in the spectrum of B films compared to Z0 films. A shifting for both organic ruthenium doped film has occurred in peaks seen at 2923, 2853, 1581, and 892 cm^{-1} of pure film.

4. Conclusions

In this study, Ru(II) complexes ([Ru(L_{1-2})(*p*-cymene)Cl]Cl) derived from perimidine ligands (L_{1-2}) were newly synthesized and used as dopant materials for produce the Ru doped ZnO thin film prepared by sol-gel spin coating. The produced thin films were characterized by using XRD, SEM, FTIR, UV, and Photoluminescence spectra. The film thicknesses were found to depend on Ru concentration and ranged from 1045 to 2586 nm. XRD analysis showed that all films had a hexagonal wurtzite structure and particle size has an increase with the rise of Ru amount. Further, the residual stresses values decreased

with the newly synthesized Ru complexes and therefore the crystalline quality increased. Also, it was found that all films had a bandgap between 2.76–3.20 eV. The PL spectra of the Ru doped ZnO films showed a strong excitation centered at 326 nm and a low intensity and broad excitation at 471, with a peak centered at around 650 nm. High excitations were found in 6% of Ru doping with A, C and B, respectively. The Ru complex of the L_1 ligand (B films) usually gave higher results compared to those with the L_2 ligand (C films). This study has shown that Ru complexes can be used in the sol-gel production of ZnO thin films, and these new high conjugated structures are promising as dopant materials for the ZnO thin film.

Declarations

Funding

The author(s) received no financial support for the research, authorship, and/or publication of this article.

Declaration of Competing Interest

The authors declare that they have no known competing financial interests or personal relationships that could have appeared to influence the work reported in this paper.

Data availability statement

The raw data required to reproduce these findings are available to download from [Insert Permanent Web Link(s)]. (Note: Permanent links will be given as mendeley data link after revisions) [52]

References

1. M. Jacobs, S. Muthukumar, A. Panneer Selvam, J. Engel Craven, **and** S. Prasad, Biosens. Bioelectron. **55**, 7 **(** (2014). https://doi.org/10.1016/j.bios.2013.11.022., **)**
2. M. Ali, N. Tit, **and** Z.H. Yamani, Int. J. Energy Res. **44**, 10926 **(** (2020). https://doi.org/10.1002/er.5656., **)**
3. X. Wang, Z. Pan, Y. Wu, X. Ding, X. Hong, G. Xu, M. Liu, Y. Zhang, **and** W. Li, Nano Res. **12**, 525 **(** (2019). https://doi.org/10.1007/s12274-018-2245-z., **)**
4. T. Nagao, T.D. Dao, R.P. Sugavaneshwar, K. Chen, **and** K.K. Nanda, Radiat. Eff. Defects Solids **171**, 22 **(** (2016). https://doi.org/10.1080/10420150.2016.1160906., **)**
5. A. Kołodziejczak-Radzimska, T. Jesionowski, Mater. (Basel) **7**, 2833 **(** (2014). https://doi.org/10.3390/ma7042833. ., **)**
6. G. Demircan, E.F. Gurses, A. Acikgoz, S. Yalcin, **and** B. Aktas, Mol. Cryst. Liq Cryst. **709**, 61 **(** (2020). https://doi.org/10.1080/15421406.2020.1816009., **)**

7. G. Demircan, S. Yalcin, K. Alivi, G. Ceyhan, A. Acikgoz, M.V. Balak, B. Aktas, **and** R. Das, Opt. Mater. (Amst) **126**, 112163 **(** (2022). https://doi.org/10.1016/j.optmat.2022.112163, **)**
8. V. Guckan, V. Altunal, A. Ozdemir, V. Tsiumra, Y. Zhydachevskyy, **and** Z. Yegingil, J. Alloys Compd. **823**, 153878 **(** (2020). https://doi.org/10.1016/j.jallcom.2020.153878., **)**
9. L. Znaidi, Mater. Sci. Eng. B **174**, 18 **(** (2010). https://doi.org/10.1016/j.mseb.2010.07.001., **)**
10. N. Bouhssira, S. Abed, E. Tomasella, J. Cellier, A. Mosbah, M.S. Aida, **and** M. Jacquet, Appl. Surf. Sci. **252**, 5594 **(** (2006). https://doi.org/10.1016/j.apsusc.2005.12.134., **)**
11. N. Kumar, A.H. Chowdhury, B. Bahrami, M.R. Khan, Q. Qiao, **and** M. Kumar, Thin Solid Films **700**, 137916 **(** (2020). https://doi.org/10.1016/j.tsf.2020.137916., **)**
12. J. Mass, P. Bhattacharya, **and** R. Katiyar, Mater. Sci. Eng. B **103**, 9 **(** (2003). https://doi.org/10.1016/S0921-5107(03)00127-2., **)**
13. M. Wang, J. Wang, W. Chen, Y. Cui, **and** L. Wang, Mater. Chem. Phys. **97**, 219 **(** (2006). https://doi.org/10.1016/j.matchemphys.2005.07.072., **)**
14. K.S. Pakhare, B.M. Sargar, R.K. Mane, **and** S.B. Wategaonkar, **Macromol**. **Symp**. 393, **2000084 (**2020**)**. https://doi.org/10.1002/masy.202000084
15. S. Mersagh Dezfuli, M. Sabzi, Appl. Phys. A **125**, 557 **(** (2019). https://doi.org/10.1007/s00339-019-2854-8., **)**
16. E. John, Oxford Univ. Press 539 **(**2001**)**
17. I. Zuba, M. Zuba, M. Piotrowski, **and** A. Pawlukojć, Appl. Radiat. Isot. **162**, 109176 **(** (2020). https://doi.org/10.1016/j.apradiso.2020.109176., **)**
18. J.-Y. Kim, K.-H. Kim, S.-B. Yoon, H.-K. Kim, S.-H. Park, **and** K.-B. Kim, Nanoscale **5**, 6804 **(** (2013). https://doi.org/10.1039/c3nr01233f., **)**
19. H. Cui, J.-H. Park, **and** J.-G. Park, J. Electrochem. Soc. **159**, H335 **(** (2012). https://doi.org/10.1149/2.103203jes., **)**. H341.
20. R. Vettumperumal, S. Kalyanaraman, **and** R. Thangavel, J. Mol. Eng. Mater. **05**, 1750004 **(** (2017). https://doi.org/10.1142/S2251237317500046., **)**
21. H. Gómez-Pozos, J. González-Vidal, G. Torres, J. Rodríguez-Baez, A. Maldonado, M. **de la Luz** Olvera, D. Acosta, M. Avendaño-Alejo, **and** L. Castañeda, **Sensors** 13, **3432 (**2013**)**. https://doi.org/10.3390/s130303432
22. J.-S. Jeng, Microelectron. Eng. **149**, 1 **(** (2016). https://doi.org/10.1016/j.mee.2015.08.014., **)**
23. F. Sarf, I. Karaduman Er, E. Yakar, **and** S. Acar, J. Mater. Sci. Mater. Electron. **31**, 10084 **(** (2020). https://doi.org/10.1007/s10854-020-03554-w., **)**
24. 19, **1 (2005). https://doi.org/10.1002/aoc.725**
25. J. Iida, E.T. Bell-Loncella, M.L. Purazo, Y. Lu, J. Dorchak, R. Clancy, J. Slavik, M. Lou, Cutler, **and** C.D. Shriver, J. Transl Med. 14, **(**2016**)**. https://doi.org/10.1186/s12967-016-0797-9
26. F. Li, J.G. Collins, **and** F.R. Keene, Chem. Soc. Rev. **44**, 2529 **(** (2015). https://doi.org/10.1039/C4CS00343H., **)**

27. A.F. Pozharskii, V.N. Koroleva, O.M. Bagrova, B.A. Semavin, **and** V.A. Bren', Chem. Heterocycl. Compd. **16**, 71 **(** (1980). https://doi.org/10.1007/BF00475397., **)**
28. A.M. Giani, M. Lamperti, A. Maspero, A. Cimino, R. Negri, G.B. Giovenzana, G. Palmisano, **and** L. Nardo, J. Lumin. **179**, 384 **(** (2016). https://doi.org/10.1016/j.jlumin.2016.07.033., **)**
29. E. Aytar, V. Kasim, Selçuk Üniversitesi Fen Fakültesi Fen Derg. **45**, 60 **(** (2019), **)**
30. E. Aytar, **Konjuge Nn Kompleks Bileşikleri ve Katalitik Uygulamaları**, 2019
31. S.C. Navale, V. Ravi, **and** I.S. Mulla, Sens. Actuators B Chem **139**, 466 **(** (2009). https://doi.org/10.1016/j.snb.2009.03.068, **)**
32. Y.-S. Choi, C.-G. Lee, **and** S. Cho, Thin Solid Films **289**, 153 **(** (1996). https://doi.org/10.1016/S0040-6090(96)08923-7., **)**
33. A. Ghosh, N. Kumari, S. Tewari, **and** A. Bhattacharjee, Mater. Sci. Eng. B **196**, 7 **(** (2015). https://doi.org/10.1016/j.mseb.2015.02.012., **)**
34. M.A. Korshunov, V.F. Shabanov, Nanotechnologies Russ. **5**, 73 **(** (2010). https://doi.org/10.1134/S1995078010010076., **)**
35. D.T. Speaks, **Int**. **J**. Mech. Mater. Eng. **15**, 2 **(** (2020). https://doi.org/10.1186/s40712-019-0113-6., **)**
36. V. Malapati, R. Singh, Int. J. Nanosci. **16**, 1650036 **(** (2017). https://doi.org/10.1142/S0219581X16500368., **)**
37. A. Kaphle, M.F. Borunda, **and** P. Hari, Mater. Sci. Semicond. Process. **84**, 131 **(** (2018). https://doi.org/10.1016/j.mssp.2018.05.019., **)**
38. A. Tuan Thanh Pham, P. Thanh Ngoc Vo, H. Kieu Thi Ta, N. Kim Pham, H. Thi Lai, H. Nhu Thi, V. Tran, T. Cao Tran **Le** Hoang Doan, S. Park, **and** T. Bach Phan, Mater. Sci. Eng. B Solid-State Mater. Adv. Technol. 261, 114712 **(**2020**)**. https://doi.org/10.1016/j.mseb.2020.114712
39. S. Al-Khawaja, B. Abdallah, S. Abou Shaker, **and** M. Kakhia, Compos. Interfaces **22**, 221 **(** (2015). https://doi.org/10.1080/15685543.2015.1002259., **)**
40. S. Liu, G. Li, M. Lan, Y. Piao, K. Miyazaki, **and** Q. Wang, Acta Crystallogr. Sect. B Struct. Sci. Cryst. Eng. Mater. **76**, 259 **(** (2020). https://doi.org/10.1107/S2052520620002383., **)**
41. S. Kumar, P. Kaur, C.L. Chen, R. Thangavel, C.L. Dong, Y.K. Ho, J.F. Lee, T.S. Chan, T.K. Chen, B.H. Mok, S.M. Rao, **and** M.K. Wu, J. Alloys Compd. **588**, 705 **(** (2014). https://doi.org/10.1016/j.jallcom.2013.11.137., **)**
42. E. Burstein, Phys. Rev. **93**, 632 **(** (1954). https://doi.org/10.1103/PhysRev.93.632., **)**
43. T.S. Moss, **Proc**. **Phys**. **Soc**. **Sect**. **B** 67, **775 (**1954**)**. https://doi.org/10.1088/0370-1301/67/10/306
44. E. Isbilir, Z. Serbetci, **and** M. Soylu, Superlattices Microstruct. **67**, 144 **(** (2014). https://doi.org/10.1016/j.spmi.2013.12.017., **)**
45. A. Galdámez-Martinez, G. Santana, F. Güell, P.R. Martínez-Alanis, **and** A. Dutt, Nanomaterials **10**, 857 **(** (2020). https://doi.org/10.3390/nano10050857., **)**
46. S. Das, U.K. Ghorai, R. Dey, C.K. Ghosh, **and** M. Pal, RSC Adv. **11**, 335 **(** (2021). https://doi.org/10.1039/D0RA04766J., **)**

47. M.M. Obeid, H.R. Jappor, K. Al-Marzoki, I.A. Al-Hydary, S.J. Edrees, **and** M.M. Shukur, RSC Adv. **9**, 33207 **(** (2019). https://doi.org/10.1039/C9RA04750F., **)**
48. A. Acikgoz, G. Demircan, D. Yılmaz, B. Aktas, S. Yalcin, **and** N. Yorulmaz, Mater. Sci. Eng. B **276**, 115519 **(** (2022). https://doi.org/10.1016/j.mseb.2021.115519, **)**
49. A. Acikgoz, G. Ceyhan, B. Aktas, S. Yalcin, **and** G. Demircan, J. Non Cryst. Solids 572, **(**2021**)**. https://doi.org/10.1016/j.jnoncrysol.2021.121104
50. R. Vinoth, S.G. Babu, V. Bharti, V. Gupta, M. Navaneethan, S.V. Bhat, C. Muthamizhchelvan, P.C. Ramamurthy, C. Sharma, D.K. Aswal, Y. Hayakawa, **and** B. Neppolian, Sci. Rep. **7**, 43133 **(** (2017). https://doi.org/10.1038/srep43133., **)**
51. P.K. Singh, N. Singh, M. Singh, S.K. Singh, **and** P. Tandon, Appl. Phys. A **126**, 321 **(** (2020). https://doi.org/10.1007/s00339-020-3439-2., **)**
52. **The reference of Data availability statement will be given as mendeley data link after revisions**

Figures

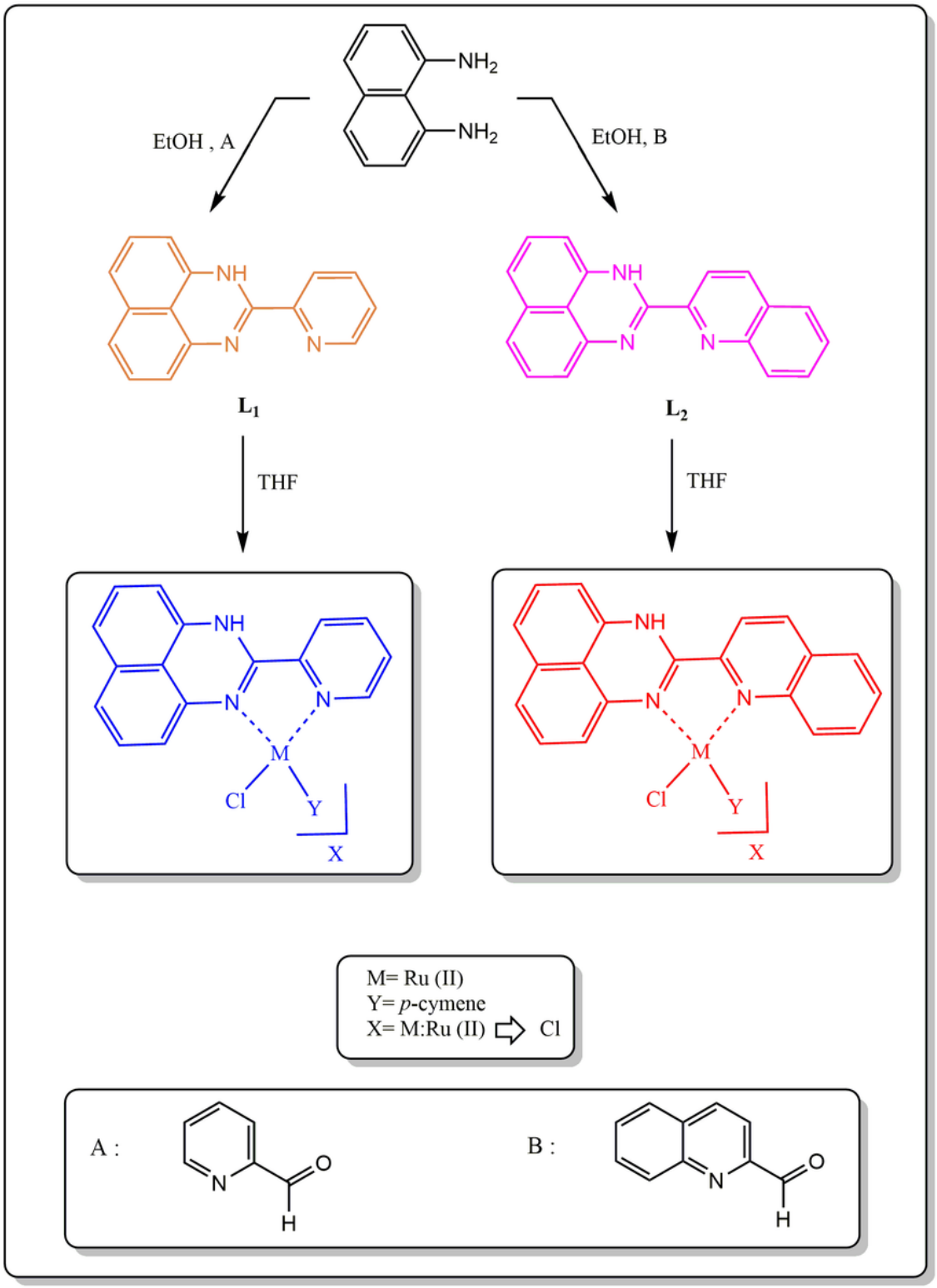

Figure 1

The structures of the proposed ligands and metal complexes

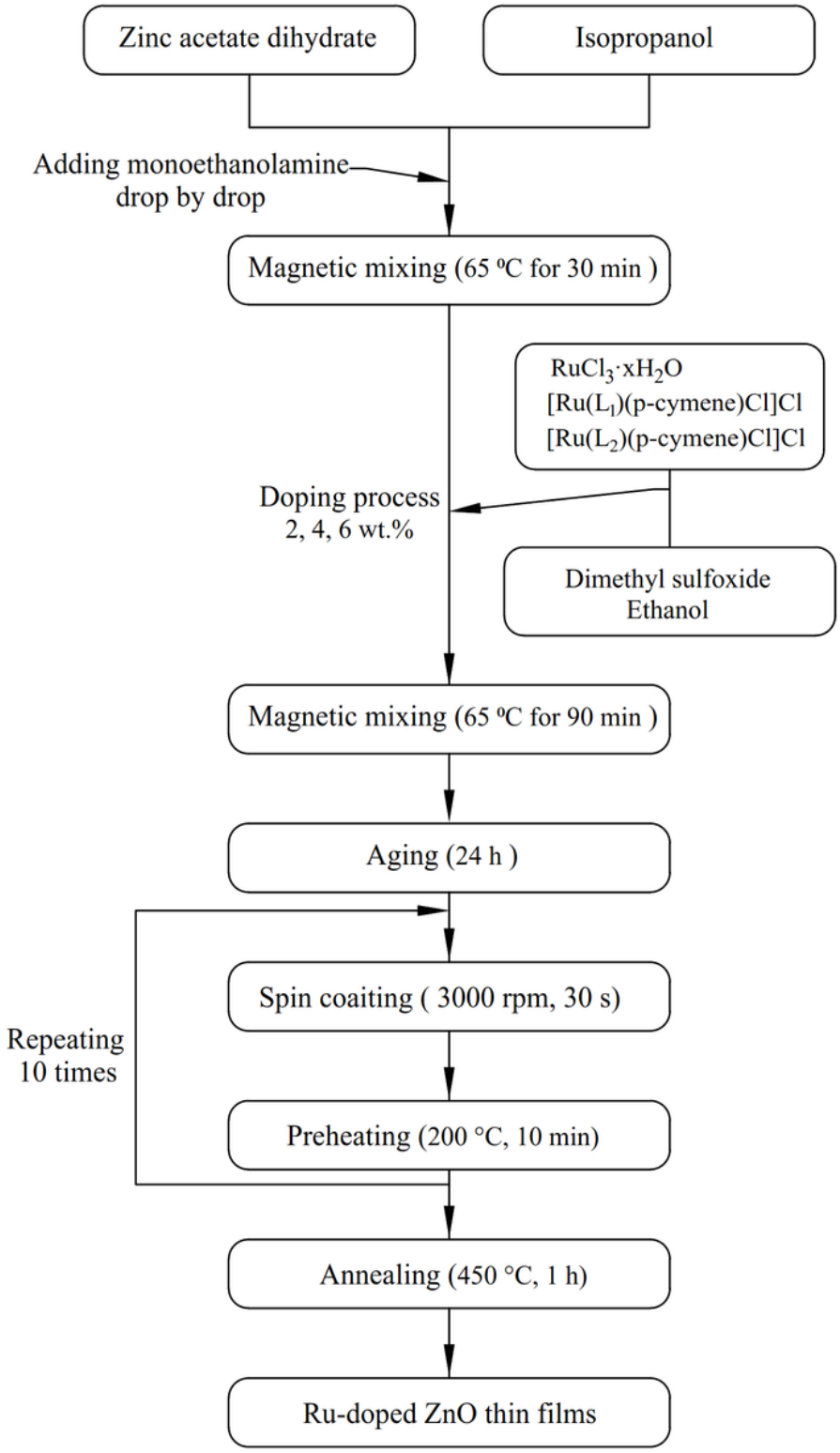

Figure 2

Flow chart of Ru-doped ZnO thin film

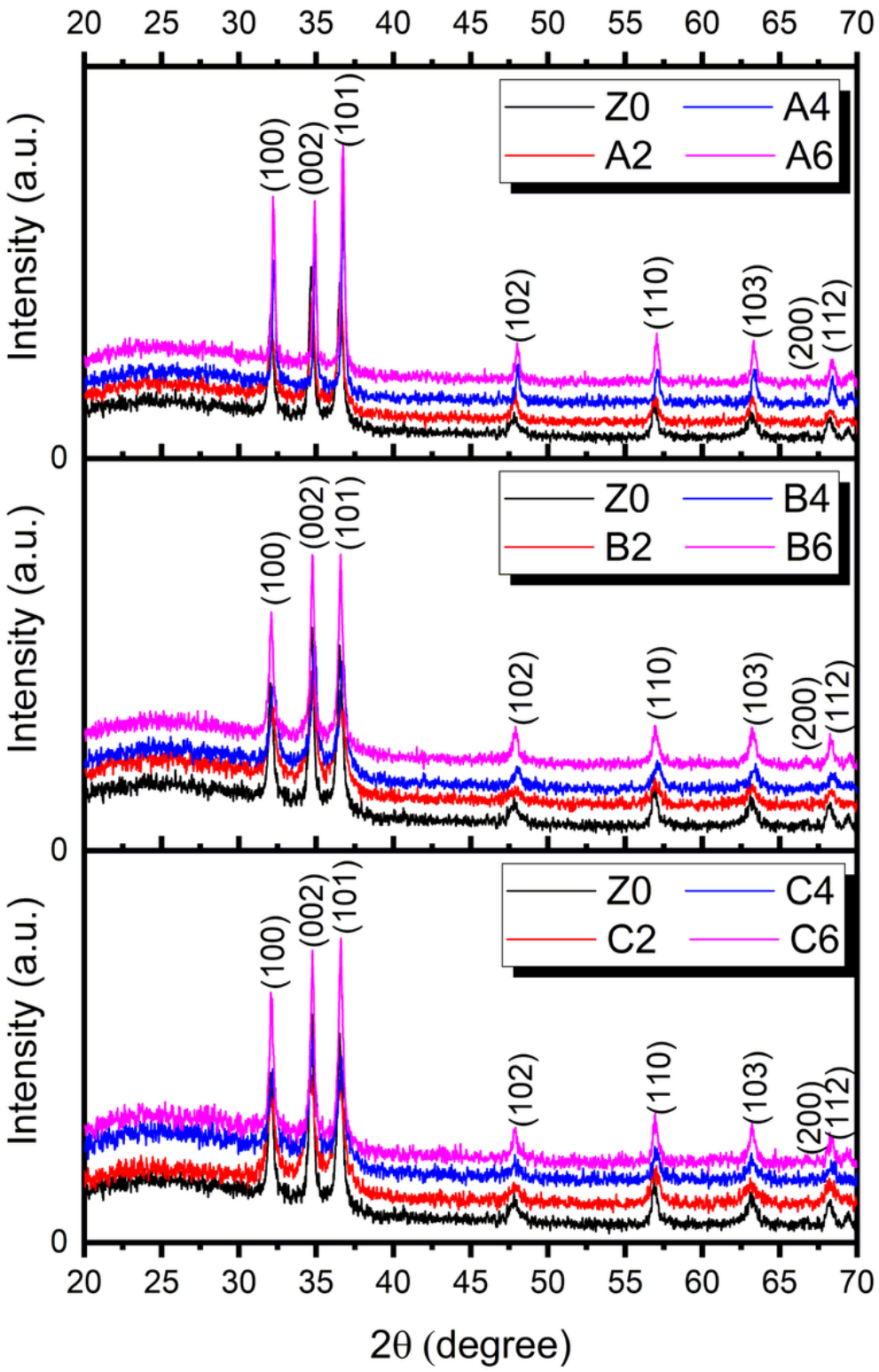

Figure 3

XRD pattern of Ru-doped ZnO thin films

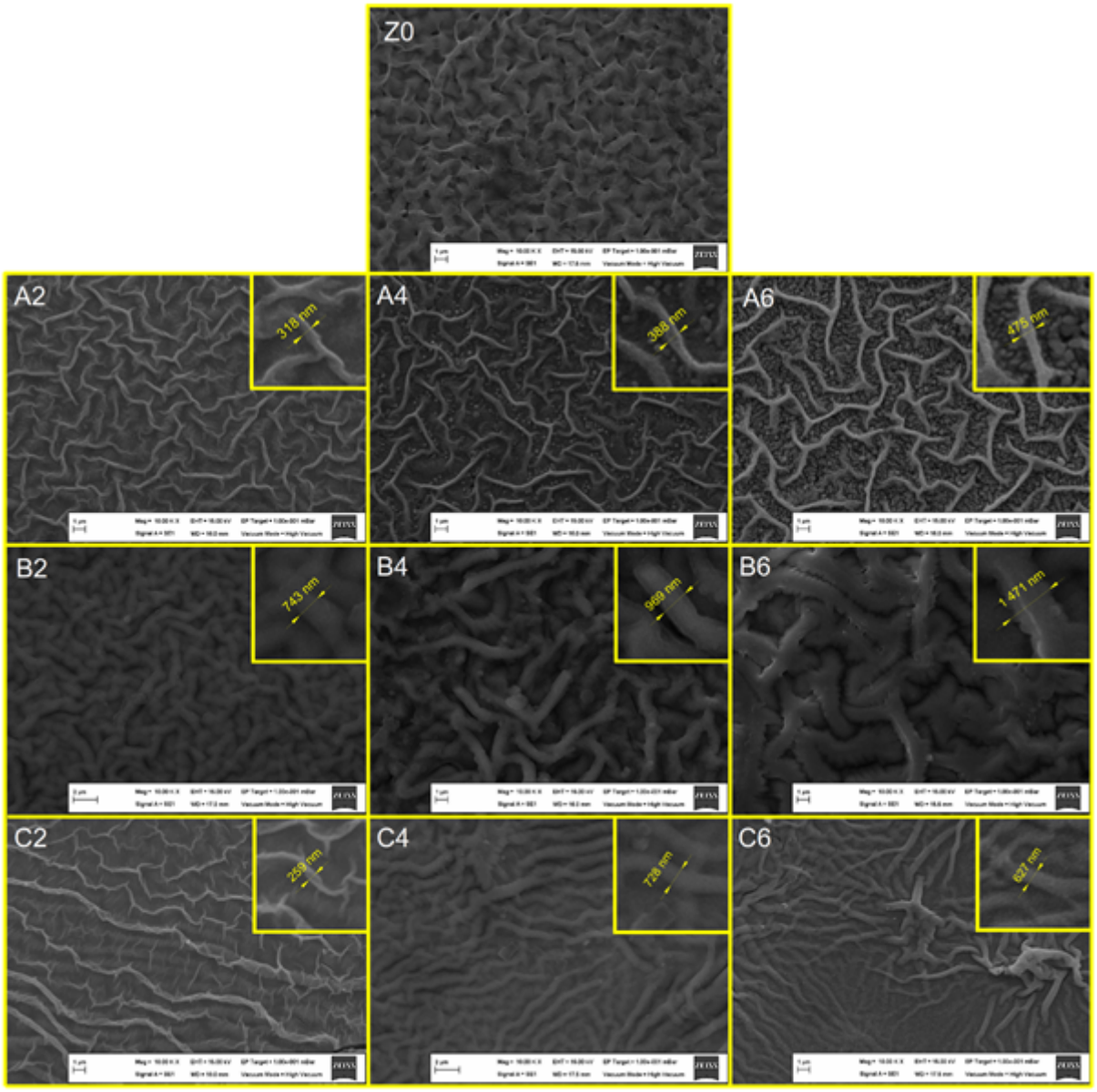

Figure 4

SEM images of Ru-doped ZnO thin films

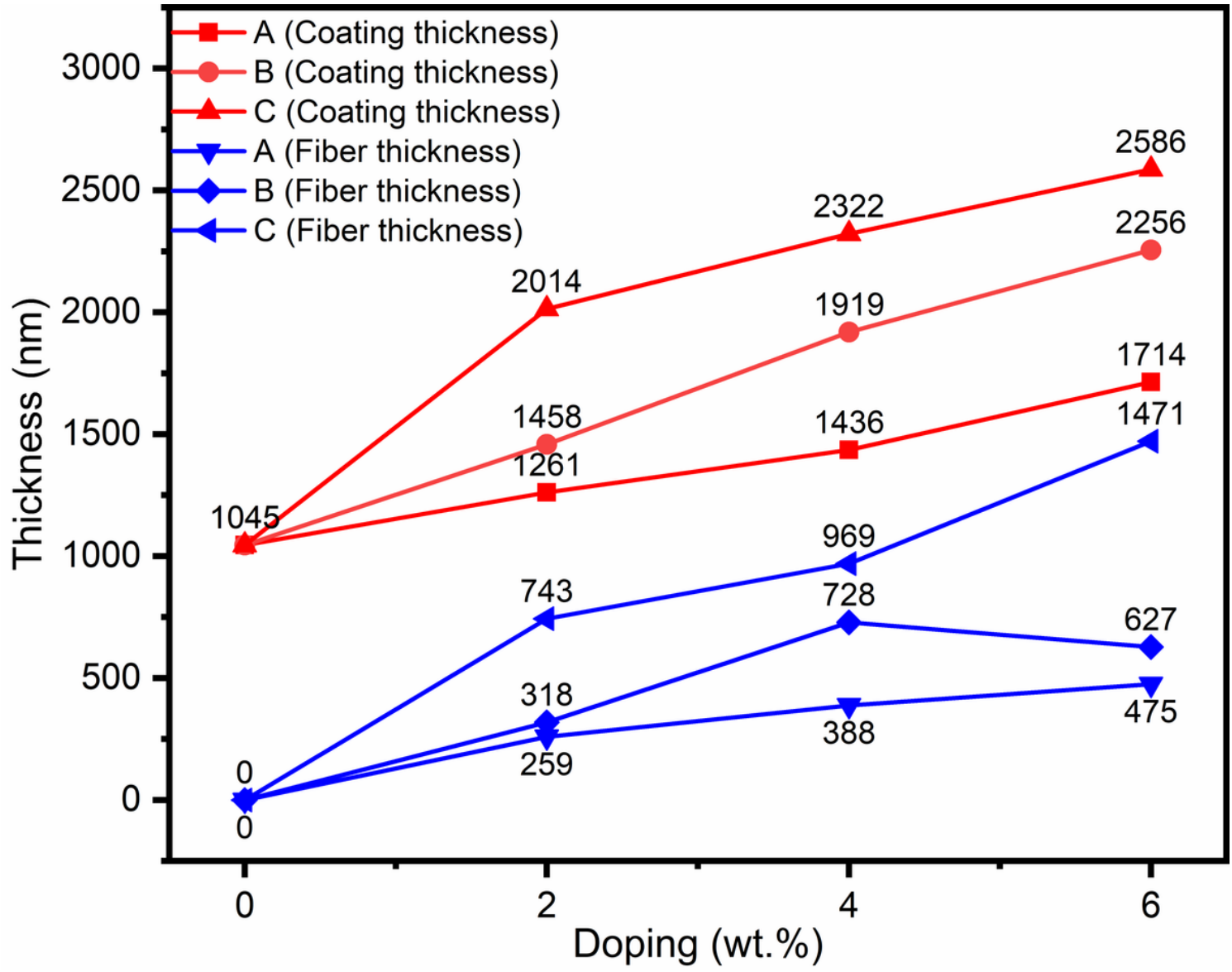

Figure 5

Coating and fiber thickness of Ru-doped ZnO thin films

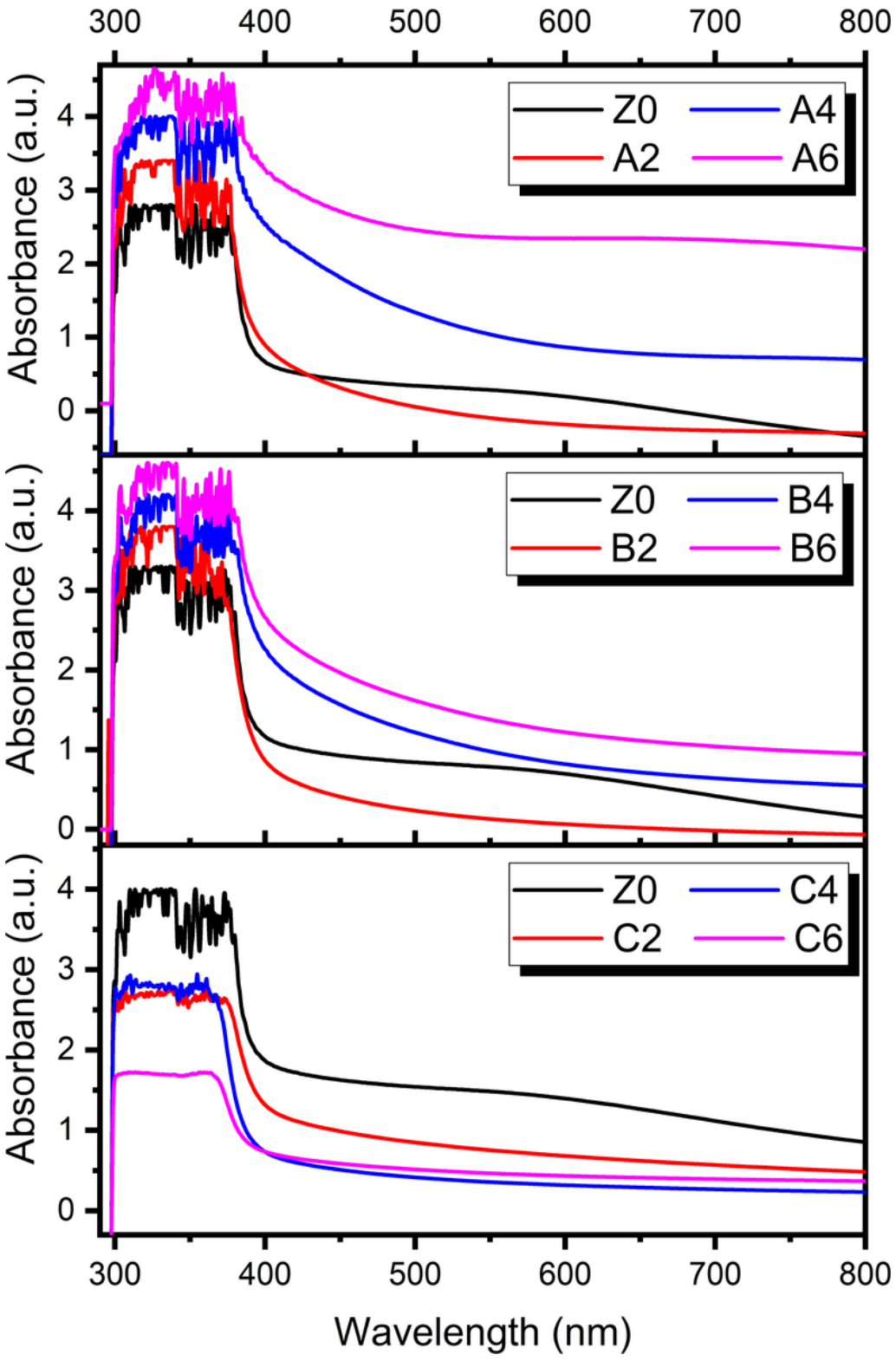

Figure 6

UV–vis absorption spectra of Ru doped ZnO thin films

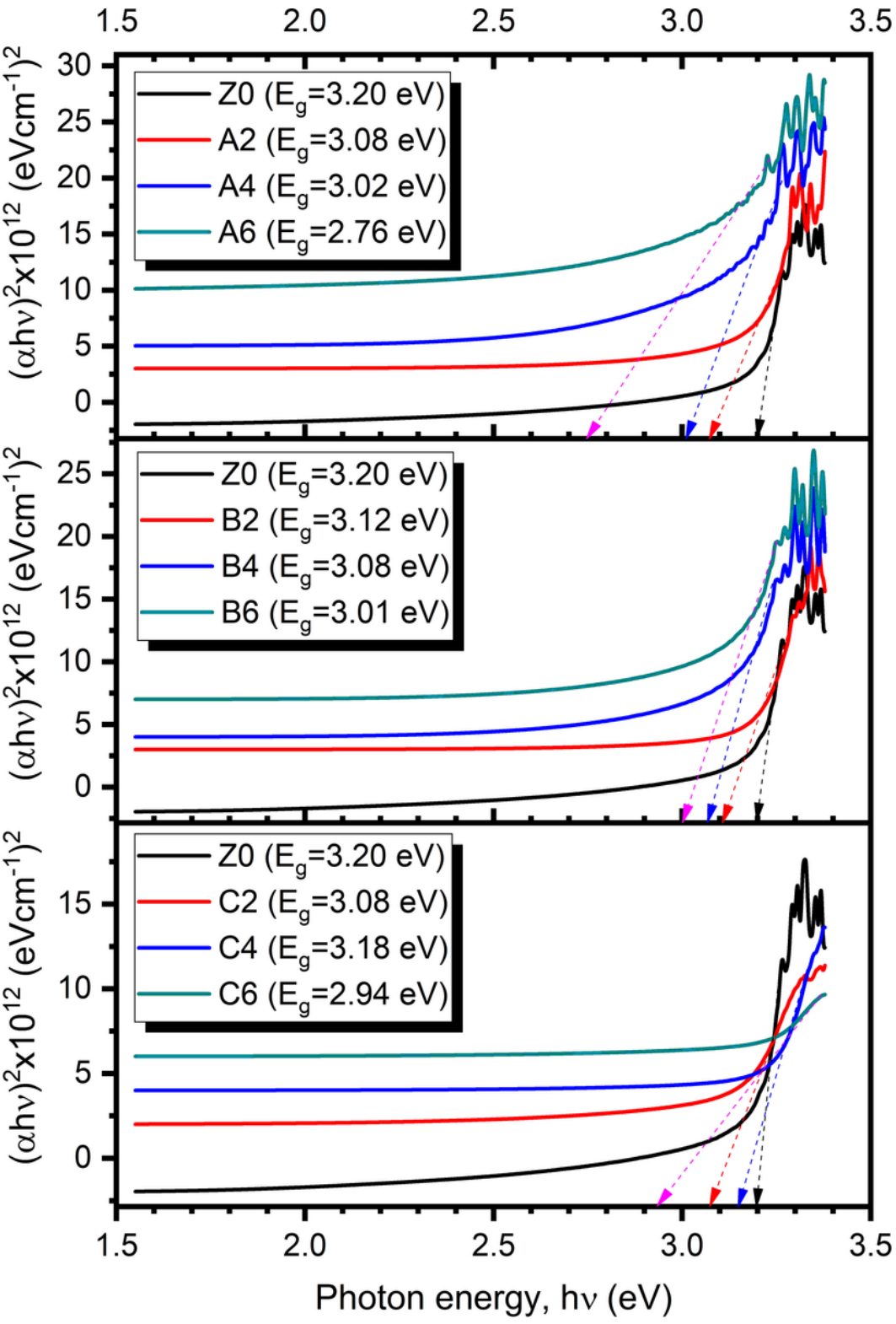

Figure 7

Optical bandgaps of Ru doped ZnO thin films

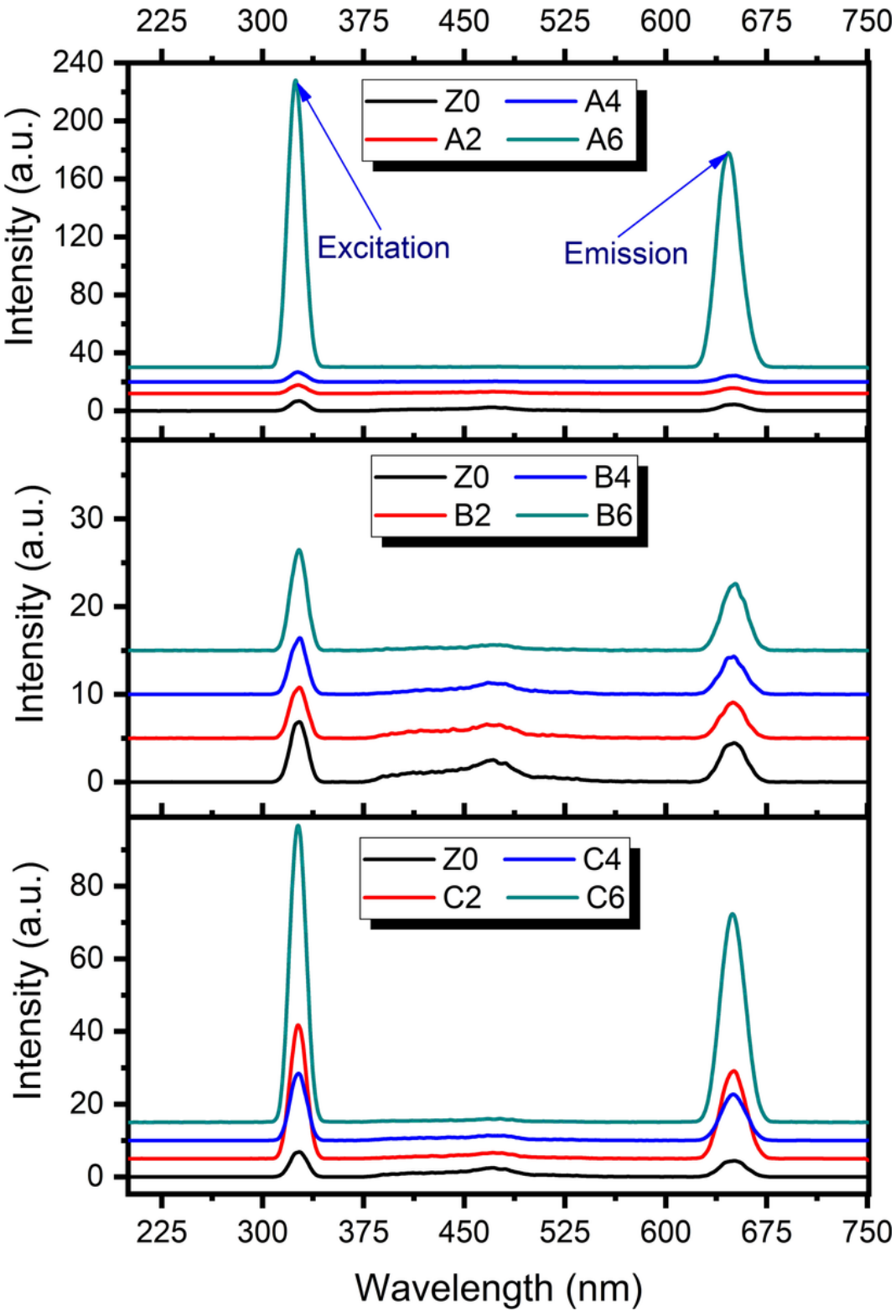

Figure 8

The Photoluminescence spectra of the Ru-ZnO thin films

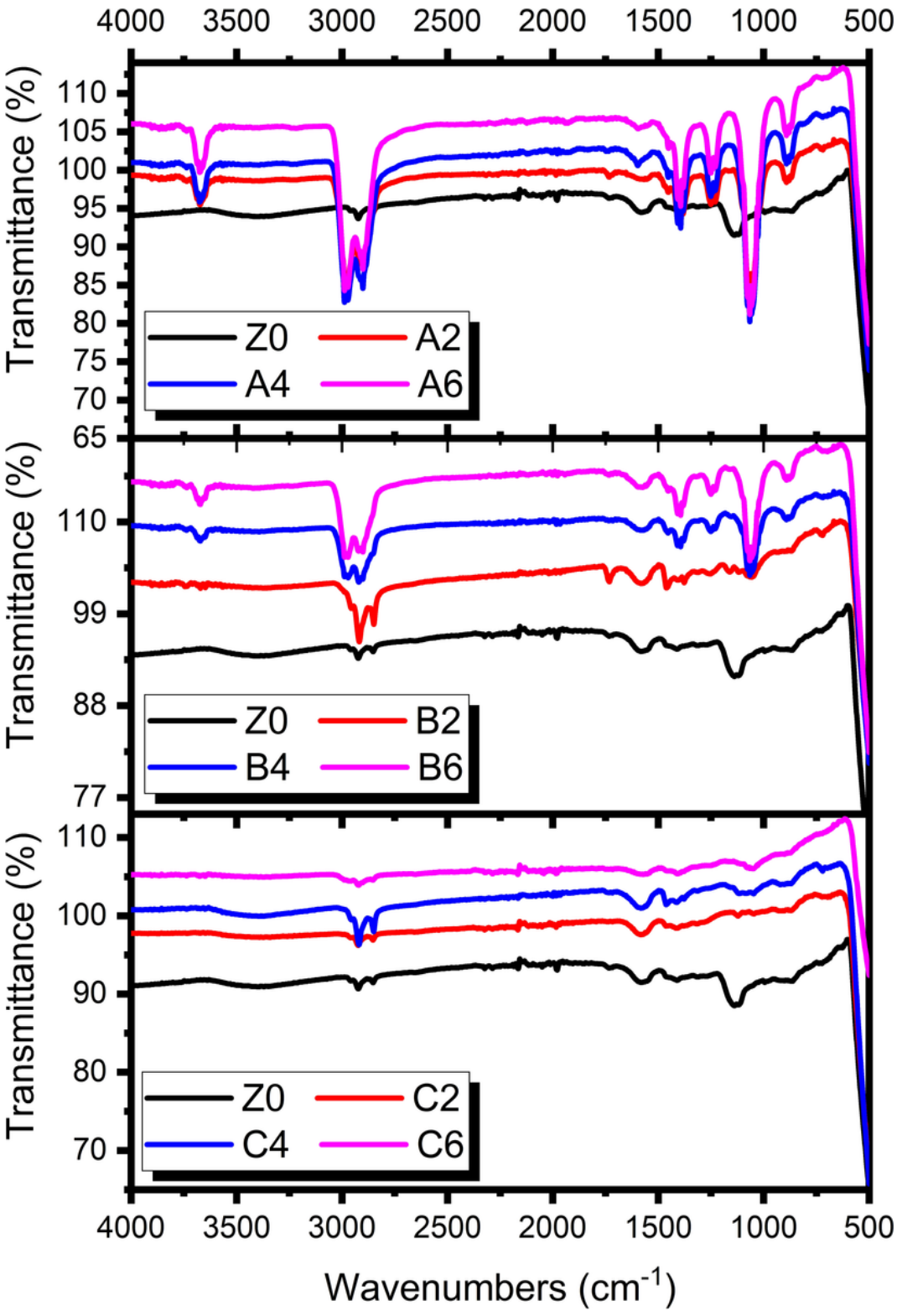

Figure 9

FT-IR analysis of Ru doped ZnO thin films

Supplementary Files

This is a list of supplementary files associated with this preprint. Click to download.

- SupportingInformationEA.docx